THE AMERICAN SOCIETY OF MECHANICAL ENGINEERS
345 E. 47 St., New York, N.Y. 10017

83-GT-134

DESIGN OF SHOCK-FREE COMPRESSOR CASCADES INCLUDING VISCOUS BOUNDARY LAYER EFFECTS

George S. Dulikravich
Assistant Professor
Department of Aerospace Engineering
and Engineering Mechanics
University of Texas at Austin
Austin ,Texas

Helmut Sobieczky
Group Leader
Institut fur Theoretische
Stroemungsmechanik
DFVLR-AVA
Goettingen, F. R. Germany

ABSTRACT

A computer code that generates shock-free transonic compressor cascade shapes while taking into account viscosity effects is developed. The mathematical model for the inviscid flow field is the full potential equation. The Kutta-Joukowski condition is satisfied by varying the free stream angle at downstream infinity. A boundary fitted computational grid of C-type is generated using a sequence of conformal mapping and nonorthogonal coordinate stretching and shearing transformations. The inviscid calculation is performed sequentially on up to four consecutively refined grids thereby accelerating the convergence of the solution process. The full potential equation is solved using a finite area technique and rotated, type-dependent finite differencing. Artificial viscosity of the first order is added in a fully conservative form. Shock-free cascade airfoil shapes are obtained using the fictitious gas concept of Sobieczky and the method of characteristics in the rheograph plane. Viscosity effects are incorporated via a boundary layer displacement thickness. The integral boundary layer code is based on Rotta's turbulence model and assumes transition region of zero length.

NOMENCLATURE

a	Speed of sound
c	Cascade airfoil maximum chord length
C	Coefficient
D	Determinant of the Jacobian: $\partial(x,y)/\partial(X,Y)$
E	Coefficient
g	Gap distance between leading edges of two neighboring airfoils in the cascade
H	Boundary layer shape factor
i	Complex number $i = \sqrt{-1}$
M	Mach number
P	Fictitious gas parameter
Q	Velocity magnitude
u,v	Velocity vector components in physical plane (x,y)
U,V	Contravariant velocity vector components in computational plane (X,Y)
$\tilde{w}$	Complex plane with (x,y) coordinates
x,y	Cartesian coordinate system; physical plane
X,Y	Coordinate system in the computational plane
$\tilde{z}$	Complex "circle" plane
$\tilde{Z}$	Complex "strip" plane
α	Free stream flow angle
β	Cascade stagger angle
γ	Ratio of specific heats
δ	Constant
ϕ	Velocity potential
ρ	Fluid density
θ,Θ^*	Momentum and energy thickness
ξ,η	Artificial (numerical) viscosity components

Subscripts

BL	boundary layer
D	drag
e	outer edge of the boundary layer
f	fictitious
F	friction
is	isentropic
LE	leading edge
n,s	locally streamline aligned cartesian coordinate system
t	artificial time
$-\infty$	upstream infinity
$+\infty$	downstream infinity
*	critical conditions

Supercripts

E central finite differencing

H upstream finite differencing

INTRODUCTION

This work represents an extension of earlier research on the design (1,2,3) and analysis of transonic shock-free cascades for compressor blade application. It has been consistently observed that very small changes in a cascade airfoil shape (particularly in regions covered by supersonic flow) can alter the entire character of the transonic cascade flow field. Changes in thickness of the same order of magnitude as the boundary layer displacement thickness can change a transonic shocked cascade flow into a transonic shockless cascade flow (2) and vice versa. Moreover, such small changes in shape can unchoke an already choked cascade (2,3).

The conclusion is that transonic cascade effects cannot be readily deduced from subsonic cascade or isolated transonic airfoil data. The most important conclusion, though, is that viscous effects must be accounted for in all transonic compressor cascade flow calculations, and results of the inviscid flow field computations alone (if done correctly) cannot be compared to experimental data. Serious doubts concerning the global aerodynamic effects of surface transpiration cooling techniques for transonic turbine cascades can also be raised. This question remains to be further investigated.

Incorporation of simplified viscous/inviscid interaction in supersonic shocked compressor cascade flow calculations has been recently performed (4). Transonic shock-free compressor cascade design with viscous/inviscid interaction was done even earlier (5). Nevertheless, that work was based on a hodograph transformation technique that often exhibits airfoil contour closure problems.

Sobieczky's fictitious gas concept (6) employed in the present work does not have closure problems, because the shock-free design starts from a given realistically shaped cascade airfoil contour.

COMPUTATIONAL GRID GENERATION

Due to the aforementioned sensitivity of transonic flows to small changes in cascade airfoil shape it is very important to apply exact boundary conditions, precisely at the surface of each airfoil. This can be easily accomplished by using boundary fitted (or boundary conforming) computational grids. Because of the periodic character of the cascade flow field it is desirable to have a geometrically periodic computational grid. Then periodicity conditions can be simply and exactly enforced without interpolating for data at the periodic grid points. When a boundary layer displacement thickness is added to the cascade airfoil contour, it is also desirable that the computational grid conform with the "open trailing edge" and the trailing wake.

A computational grid of the periodic C-type (7) offers all of the aforementioned advantages. C-type grids can be generated so that grid lines of the two basic families intersect at right angles. This is somewhat complicated and time consuming. Because a finite area technique will be used for the flow computations in this work, the grid does not have to possess strict orthogonality. The following technique offers an economical way to generate such cascade grids.

A periodic strip of the cascade flow field is conformally mapped onto a unit circle which is then conformally transformed onto a finite length strip. The airfoil contour thus maps onto a deformed unit circle and consequently onto an irregular lower boundary of the strip. With increasing cascade stagger angle the strip assumes an increasingly distorted rhomboidal shape. Such an irregular domain is then transformed to a rectangular computational plane using separate nonlinear coordinate shearing and stretching transformations. This exceptionally fast and simple cascade grid generation technique has already been extended to three-dimensional realistic geometries (8,9).

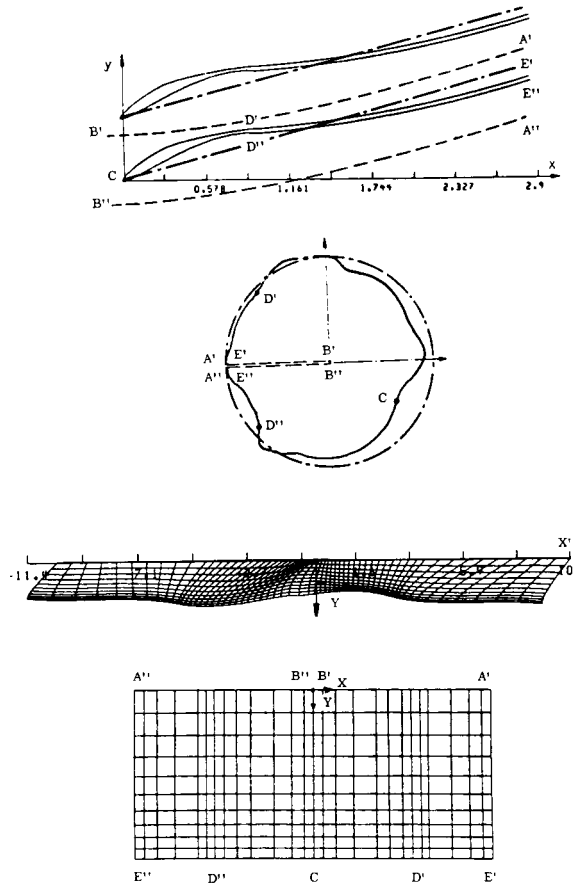

FIG. 1 THE GLOBAL GRID GENERATION/TRANSFORMATION SEQUENCE

The global transformation sequence is sketched in Fig. 1 where the complex mapping functions are (7)

$$\tilde{w} = \tilde{w}_{LE} + \frac{g}{2\pi}\{e^{i\beta}[2\beta\sin\beta + 2\cos\beta\ \ell n\ (\frac{2\cos\beta}{1-\tilde{z}})] + (\ell n\tilde{z} - i\pi)\} \quad (1)$$

and

$$\tilde{Z} = [\ell n\ (\frac{1+\tilde{z}}{1-\tilde{z}})]^{1/2} \quad (2)$$

An example of a C-type grid for a realistically shaped compressor cascade with included wake is shown in Fig.

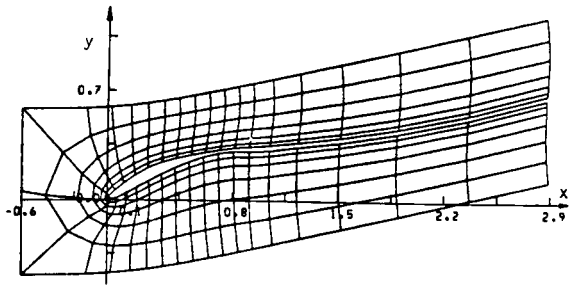

FIG. 2 C-TYPE GRID FOR A STAGGERED COMPRESSOR CASCADE WITH INCLUDED WAKE

FLOW ANALYSIS OF EXISTING CASCADES

As already mentioned, the mathematical model for the flow field dynamics used in this work is the full potential equation (10)

$$\rho\{(1-\frac{\phi_x^2}{a^2})\phi_{xx} - \frac{2\phi_x\phi_y}{a^2}\phi_{xy} + (1-\frac{\phi_y^2}{a^2})\phi_{yy}\} = 0 \qquad (3)$$

It is easily shown that this second-order quasi-linear partial differential equation can be rewritten in its most concise (canonical) form as (10,11)

$$\rho\{(1 - M^2)\phi_{ss} + \phi_{nn}\} = 0 \qquad (4)$$

where (s,n) is the cartesian coordinate system locally aligned with the streamline direction s. Eqs. (3) and (4) represent two nonconservative forms of mass conservation

$$\vec{\nabla} \cdot (\rho\vec{Q}) = (\rho u)_x + (\rho v)_y = 0 \qquad (5)$$

for planar, steady, homentropic, irrotational flow of an inviscid, ideal fluid. Eq. (5) rather than Eq. (3) or Eq. (4) should be satisfied in transonic shocked flow computations because Eq. (5) is in the fully conservative (divergence free) form and as such it accepts discontinuities in its solution. These discontinuities must not generate any vorticity in the flow field. Those isentropic shocks are characterized by the fact that they satisfy mass conservation, but do not satisfy the momentum equation. Therefore the strengths and locations of the isentropic shocks differ (2) from strengths and locations of Rankine-Hugoniot shocks. Eq. (5) is a steady-state equation. For the purpose of constructing an iterative scheme for its numerical solution Eq. (5) needs to be (at least artificially) time dependent (11,12). Besides, it is important to note that the nonconservative equivalents of Eq. (5) (that is, Eq. (3) and Eq. (4)) change their basic character from elliptic to hyperbolic form as the flow locally changes from subsonic to supersonic respectively. These two basic types of partial differential equations have their specifically shaped local domains of dependence. In order to numerically mimic these analytic domains of dependence we use type-dependent (13) finite differencing applied to second derivatives of ϕ only.

Thus, at all the grid points of the discretized flow field where the flow is locally subsonic we are actually solving

$$\rho\{[(1 - \frac{\phi_x^2}{a^2})\phi_{xx}^E - \frac{2\phi_x\phi_y}{a^2}\phi_{xy}^E + (1 - \frac{\phi_y^2}{a^2})\phi_{yy}^E] + [C_1\phi_{xt} + C_2\phi_{yt} + C_3\phi_t]\} = 0 \qquad (6)$$

Superscript E designates central differencing used, while the mixed space-artifical time terms are formed from the combination of old and new values of ϕ after each iterative sweep through the flow field.

At those grid points where the flow is locally supersonic we use upstream differencing: The word upstream having its literal meaning that is obvious from the form of the equation actually being discretized at the supersonic points

$$\rho\{[(1 - M^2)\phi_{ss}^H + \phi_{nn}^E] + [\xi_x^H + \eta_y^H] + [\delta_1\phi_{st} + \delta_2\phi_{nt} + C_3\phi_t]\} = 0 \qquad (7)$$

Superscript H here designates upstream differencing and the terms ξ and η are the artificial or numerical viscosity terms introduced to cancel the error introduced by upstream rotated differencing (11) applied to ϕ_{ss} term only. Note that Eq. (7) can be rewritten in its partially conservative form as

$$\rho\{[(\rho u)^E + \xi^H]_x + [(\rho v)^E + \eta^H]_y + [\delta_1\phi_{st} + \delta_2\phi_{nt} + C_3\phi_t]\} = 0 \qquad (8)$$

After a large number of iterations the artificially time dependent terms will vanish. The artificial viscosity or dissipation terms ξ and η tend to zero with the refinement of the computational grid if they are introduced in a fully conservative form. This should guarantee the ability of the numerical scheme to uniquely capture the isentropic shocks (14). Nevertheless, it has been observed by the authors of this work as well as by other researchers (15,16,17) that the uniqueness of the isentropic shock strength and location are not fully guaranteed by this numerical scheme. Further research into the acceptable forms for ξ and η artificial dissipation terms is still necessary.

The finite area technique (14) used in this work actually represents finite differencing performed in a uniformly discretized rectangular (Fig. 1) computational plane (X,Y). Besides transforming the computational grid from the physical plane (x,y) to the computational plane (X,Y) it is necessary also to transform the governing equation and the boundary conditions. This is easily done using the contravariant velocity vector component notation

$$\begin{Bmatrix} U \\ V \end{Bmatrix} = \begin{bmatrix} x_X & x_Y \\ y_X & y_Y \end{bmatrix}^{-1} \begin{Bmatrix} u \\ v \end{Bmatrix} \qquad (9)$$

Then the mass conservation equation (with artificial dissipation included) in its steady conservative form becomes

$$\frac{1}{D}\{[(\rho DU)^E + \bar{\xi}^H]_X + [(\rho DV)^E + \bar{\eta}^H]_Y\} = 0 \qquad (10)$$

where

$$D = x_X y_Y - x_Y y_X \tag{11}$$

The boundary condition on the airfoil surface then becomes

$$V = 0 \tag{12}$$

Uniform flow conditions are enforced at the upstream and downstream flow field boundary.

SHOCK-FREE REDESIGN OF EXISTING CASCADES

Isentropic compression shocks are possible only when a locally hyperbolic full potential equation just ahead of the shock changes to a locally elliptic full potential equation just behind the shock. It follows that for an isentropic shock to exist at all it is absolutely necessary that the full potential equation be at least locally of a hyperbolic type. Hence for an isentropic shock not to exist at any point in a flow field the problem is to be formulated so that the governing full potential equation never becomes hyperbolic at any point in the flow field.

This is obviously not possible if isentropic relations for the speed of sound

$$\frac{a_{is}^2}{a_*^2} = \frac{\gamma+1}{2} - \frac{\gamma-1}{2} M_*^2 \tag{13}$$

and for the fluid density

$$\frac{\rho_{is}}{\rho_*} = \left(\frac{\gamma+1}{2} - \frac{\gamma-1}{2} M_*^2\right)^{1/(\gamma-1)} \tag{14}$$

are used at every point of the flow field. But, if one uses isentropic relations (Eqs. (13) and (14)) only at the points where the flow is locally subsonic (including the locally sonic flow, that is, $M_* = 1.0$) and then switches to certain non-isentropic (fictitious) relations whenever the flow is locally supersonic, the governing full potential equation will remain elliptic and the shockless flow conditions will be satisfied at every grid point of the flow field. This is the basic idea behind Sobieczky's fictitious gas concept (6) that has successfully been applied to shock-free flow field redesign of existing shocked transonic isolated airfoils (18), isolated wings (19), two-dimensional compressor cascades (1,2,3) and quasi-three-dimensional compressor cascades (20).

Analytic expressions that could be used for the calculation of fictitious density and fictitious speed of sound are not completely arbitrary. They must satisfy a number of general constraints (1,2) in order to assure that the full potential equation will retain its elliptic character even inside the supercritical zones. The most important condition that an analytic function for the fictitious density must satisfy is that it maintains (continuously) the elliptic character of the full potential equation. The borderline between the hyperbolic and elliptic character of the full potential equation is characterized by the parabolicity (sonic) flow condition, that is,

$$\frac{\rho_f}{\rho_*} = \frac{1}{M_*} \tag{15}$$

The domain of possible analytic expressions for the ficitious density is shown in Fig. 3.

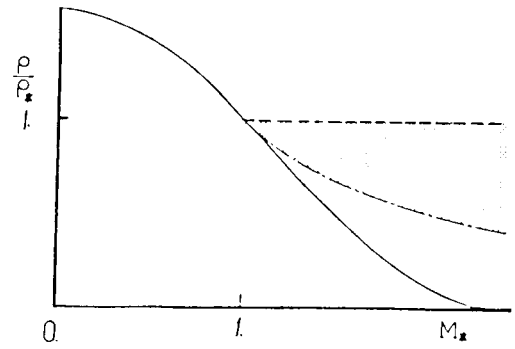

FIG. 3 ISENTROPIC DENSITY (FULL LINE), PARABOLIC LIMIT (DOTTED LINE) AND FICTITIOUS DENSITY DOMAIN (SHADED REGION)

In the present work we used the following expression

$$\frac{\rho_f}{\rho_*} = [1 + (M_* - 1)(2P - 1)]^{-1/(2P-1)} \tag{16}$$

Note that when the input parameter $P = 1$, Eq. (16) is equal to Eq. (15) for $M_* = 1$. That is, flow parameters iteratively calculated at the points on a sonic line are correct because they satisfy not only fictitious relations, but also exact isentropic relations. Fictitious speed of sound can be found from the general expression (1,2,21)

$$\frac{a_f^2}{a_*^2} = -M_* \left(\frac{\rho_f}{\rho_*}\right) \Big/ \frac{d}{dM_*}\left(\frac{\rho_f}{\rho_*}\right) \tag{17}$$

In such a way we determined a sonic line shape that is compatible with a shock-free flow field. The final question is: what is the new shape of the airfoil in the cascade that will produce such a flow field.

Subsonic portions of the flow field are already correctly computed because the isentropic relations (Eqs. (13) and (14)) were used there. Hence, only the portions of the airfoil contour that are covered by the supersonic flow need to be modified. The sonic lines and the subsonic portions of the flow field are not to be altered if this modification is performed correctly.

Each supersonic zone is bounded with a sonic line and a part of the airfoil surface. If correct (isentropic) relations are used throughout the flow field the shape of the boundaries of each supersonic zone will have to be changed to accommodate the ideal fluid (Eqs. (13) and (14)) rather then the fictitious fluid (Eqs. (16) and (17)) flow. Sonic lines need to be kept intact in order to secure an entirely shock-free flow field. This means that the airfoil shape must be changed in each region where it is covered by the local supersonic zone.

Using isentropic relations inside each supersonic zone will result in an initial-value problem governed by a strictly hyperbolic full potential equation. The initial values are known on the sonic line (potential function - hence stream function) and the problem is most effectively solved using the method of characteristics. To simplify this task even further, the method of characteristics is performed in a rheograph plane (6) where the full potential equation becomes linear and the two families of characteristics are

straight, mutually orthogonal lines. Once the characteristics integration is numerically performed inside each supersonic zone, the new airfoil contour is determined from the condition that the stream function must have the same value at every point of the airfoil contour.

When a check-up analysis computation is performed on such a partially redesigned cascade of airfoils (using now isentropic relations at every point of the flow field) the resulting sonic lines should be identical with the sonic lines that were obtained with the fictitious relations (Eqs. (16) and (17)) in supersonic regions and the original cascade airfoil shape.

BOUNDARY LAYER EFFECTS

Different concepts exist for an effective treatment of the interaction between viscous boundary layer and inviscid outer flow. The present work utilizes the straightforward boundary layer displacement thickness as an effective airfoil surface displacement parameter. A different approach utilizes a semi-inverse method (22) where the boundary layer is calculated from a prescribed streamwise gradient of the displacement thickness. The inviscid flow field is then recomputed with such a modified airfoil shape thus completing one iterative cycle of the global viscous/inviscid computation loop.

In this work the computational procedure starts with an initial guess (23) for the displacement thickness

$$\delta^* = c \sum_{n=1}^{N} C_{BLn} \left(\frac{x}{c}\right)^{E_{BLn}} \qquad (18)$$

The displacement thickness, δ^*, is normally added to the airfoil contour and the resulting shape is analysed by the full potential (inviscid) part of the computer code (24). With the output from the inviscid computation the boundary layer displacement thickness is recomputed using Rotta's integral dissipation method (25,26) code. This code solves simultaneously, von Karman's momentum equation

$$\frac{d\theta}{ds} + \theta\left[\frac{H+2}{Q_e}\frac{dQ_e}{ds} + \frac{1}{\rho_e}\frac{d\rho_e}{ds}\right] = \frac{C_F}{2} \qquad (19)$$

and the energy equation

$$\frac{d\theta^*}{ds} + \theta^*\left[\frac{3}{Q_e}\frac{dQ_e}{ds} + (2-\gamma)\frac{1}{\rho_e}\frac{d\rho_e}{ds}\right] = C_D \qquad (20)$$

while utilizing several additional relations determining H, the shape factor; C_f, the skin friction coefficient; and C_D, the dissipation coefficient. If the boundary layer thickness values resulting from this code are found to be close to the analytically obtained values (Eq. (18)), the latter are then subtracted (normally) from the thickened cascade airfoil contour and the resulting airfoil shape should be the one that can be machined.

RESULTS

A cascade of compressor-type airfoils was generated using an analytic function (24) and an analytically controllable "bump" was added on the suction surface. The initial guess for the boundary layer displacement thickness function was obtained from Eq. (18) by choosing suitable parameters corrected iteratively.

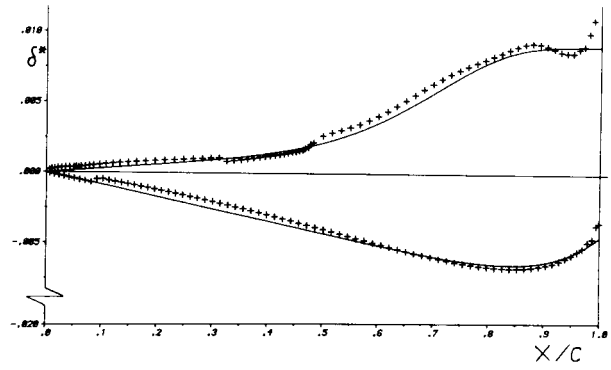

FIG. 4 BOUNDARY LAYER DISPLACEMENT THICKNESS ON UPPER AND LOWER SURFACE OF THE CASCADE AIRFOIL: (—) ANALYTICAL MODEL (EQ. (18)):(+) COMPUTED AFTER FULL POTENTIAL SHOCKLESS DESIGN COMPUTATION

Chordwise distribution of the final displacement thickness model is shown in Fig. 4. These values were added to the original cascade airfoil contour and this "thickened" shape was submitted to the shock-free redesign portion of the code. Four-level computational grid refinement was used to accelerate the convergence. The resulting shock-free airfoil shape is shown in Fig. 5 together with the characteristics grid inside the supersonic bubble.

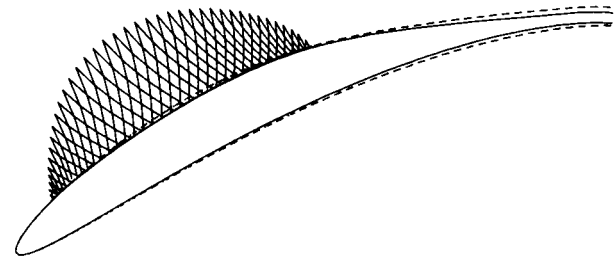

FIG. 5 ORIGINAL CASCADE AIRFOIL CONTOUR WITH A MODELED BOUNDARY LAYER DISPLACEMENT THICKNESS (---) AND THE REDESIGNED SHOCK-FREE AIRFOIL CONTOUR (—) AFTER BOUNDARY LAYER DISPLACEMENT THICKNESS SUBTRACTION AND THE FICTITIOUS GAS AIRFOIL CONTOUR MODIFICATION

The "thickened" contour is indicated here by a dotted line. Note that the amount of "shaving" that was performed by the shock-free redesign procedure is very small indeed. The boundary layer displacement thickness that was computed with Rotta's boundary layer code is shown in Fig. 4. This thickness agrees well with the modeled values except on the upper surface close to the trailing edge where the results of the boundary layer computation are unreliable and the displacement is modeled on wind tunnel boundary layer measurements (27). From Fig. 4 it can be concluded that the transition in the boundary layer occurred at approximately 46% of the chord on the suction surface and at about 9% of the chord on the pressure surface, with a slight separation at the trailing edge on the suction surface.

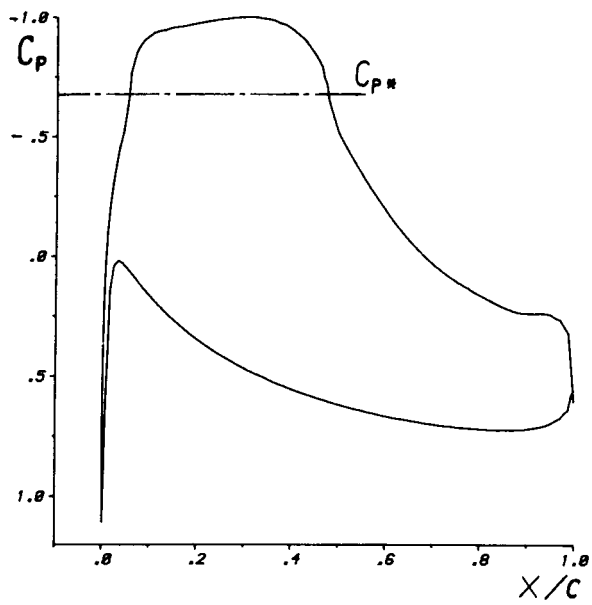

FIG. 6 COEFFICIENT OF PRESSURE DISTRIBUTION FOR THE REDESIGNED (SHOCK-FREE) CASCADE AIRFOIL WITH BOUNDARY LAYER INCLUDED

The final plot of the coefficient of pressure distribution (Fig. 6) shows that the redesigned airfoil is really shock-free and with a heavy aft loading. The cascade global parameters were: M_{∞} = 0.73; g/c = 1.1; β = 27.3°; $\alpha_{-\infty}$ = 43°; $\alpha_{+\infty}$ = 17°.

CONCLUSION

A new computer code, CAS24, has been developed and successfully applied to shockless redesign of transonic compressor planar cascades accounting for boundary layer effects. A computational grid of C-type was generated in a very efficient way using analytic transformations. Inviscid flow field computations were performed using a finite area technique, and the shock-free flow field redesign procedure utilized Sobieczky's fictitious gas concept and the method of characteristics. A boundary layer displacement thickness was analytically modeled and subtracted from an already pre-thickened and shock-free shaved airfoil contour. Rotta's integral method boundary layer code was used for controlling the analytic model. The resulting airfoil surface is slightly thinner in the region covered by the locally supersonic shock-free flow.

ACKNOWLEDGMENT

The authors express their gratitude to their respective institutions and to NASA Lewis Research Center, Computational Fluid Mechanics Branch for supporting this research project.

REFERENCES

1. Dulikravich, D.S. and Sobieczky, H., "Shockless Design and Analysis of Transonic Blade Shapes," AIAA Paper No. 81-1237 presented at the 14th AIAA Fluid Plasma Dynamics Conference, Palo Alto, California, June 23-25, 1981; also NASA TM 82611, 1981

2. Dulikravich, D.S. and Sobieczky, H., "CAS22-Fortran Program for Fast Design and Analysis of Shock Free Airfoil Cascades," NASA CR 3507, 1982.

3. Sobieczky, H. and Dulikravich, D.S., "A Computational Design Method for Transonic Turbomachinery Cascades," ASME Paper No. 82-GT-117 presented at the 27 International Gas Turbine Conference, London, Great Britain, April 18-22, 1982.

4. Calvert, W.J., "An Inviscid-Viscous Interaction Treatment to Predict the Blade-to-Blade Performance of Axial Compressors with Leading Edge Normal Shock Waves," ASME Paper 82-GT-135, London, Great Britain, 1982.

5. Korn, D., "Numerical Design of Transonic Cascades," Courant Institute of Mathematical Sciences, ERDA Research and Development Report COO-3077-72, January 1975, New York.

6. Sobieczky, H., "Transonic Fluid Dynamics-Lecture Notes," The University of Arizona, TFD 77-01, October 1977.

7. Sockol, P., "Generation of C-Type Grids for Viscous Flow Computation," Numerical Grid Generation Techniques, NASA CP-2166, 1980, pp. 437-448.

8. Dulikravich, D.S., "Fast Generation of Three-Dimensional Computational Boundary Conforming Periodic ' rids of C-type," presented at the Symposium on Numerical Generation of Curvilinear Coordinate Systems and use in the Numerical Solution of Partial Differential Equations, Nashville, Tennessee, April 13-16, 1982; also NASA CR 165596, 1982.

9. Dulikravich, D.S., "GRID3C-Computer Program for Generation of C-Type Multilevel, Three-Dimensional, Boundary Conforming Periodic Grids," NASA CR 167846, 1982.

10. Von Mises, R., "Mathematical Theory of Compressible Fluid Flow," Academic Press, Inc., New York, 1958, page 241.

11. Jameson, A., "Transonic Flow Calculations," in Computational Fluid Dynamics, Vol. 1, Von Karman Institute, VKI-LS-87-VOL-1, 1976, pp. 1.1-5.84.

12. Garabedian, P.R., "Estimation of the Relaxation Factor for Small Mesh Sizes," Math. Tables & Aids to Comput., Vol. 10, 1956, pp. 183-185.

13. Murman, E.M. and Cole, J., "Calculation of Plane Steady Transonic Flows." AIAA Journal, Vol. 9, 1971, pp. 114-121.

14. Jameson, A. and Caughey, D.A., "A Finite Volume Scheme for Transonic Potential Flow Calculations," AIAA Paper 77-635, 1977.

15. Chen, L.-T. and Caughey, D.A., "On Various Treatment of Potential Equations at Shocks," in Numerical Boundary Condition Procedures, NASA CP 2201, 1981, pp. 121-138.

16. Caspar, J.R., "Unconditionally Stable Calculation of Transonic Potential Flow Through Cascades Using an Adaptive Mesh for Shock Capture," ASME Paper No. 82-GT-238.

17. Ecer, A. and Akay, H.U., "Finite Element Analysis of Transonic Flows in Cascades - Importance of Computational Grids in Improving Accuracy and Convergence," NASA CR3446, 1981.

18. Sobieczky, H., "Related Analytical, Analog and Numerical Methods in Transonic Airfoil Design," AIAA Paper No. 79-1556, 1979.

19. Sobieczky, H., Fung, K-Y., Yu, N. and Seebass, R., "A New Method for Designing Shock-Free Transonic Configurations," AIAA Journal, Vol. 17, No. 7, July 1979, pp. 722-729.

20. Beauchamp, P., "A Numerical Tool for the Design of Shock-Free Transonic Cascades," M.Sc. Thesis, Aerospace Engineering Department, University of Arizona, Tucson, AZ., June 1981.

21. Fung, K-Y., Sobieczky, H. and Seebass, R., "Numerical Aspects of the Design of Shock-Free Wings," AIAA Paper No. 79-1557, 1979.

22. Wigton, L.B. and Holt, M., "Viscous-Inviscid Interaction in Transonic Flow," AIAA Paper No. 81-1003, 1981.

23. Sobieczky, H., "Design of Advanced Technology Transonic Airfoils and Wings," Subsonic/Transonic Configuration Aerodynamics, AGARD Fluid Dynamics Panel Symposium, AGARD CP-285, 1980.

24. Dulikravich, D.S. and Sobieczky, H., "CAS24-Fortran Program for Shock-Free Design and Analysis of Turbomachinery Cascades Including Viscous/Inviscid Effects," to appear as NASA CR, 1983.

25. Rotta, J.C., "Turbulent Boundary Layer Calculations with the Integral Dissipation Method," Computation of Turbulent Boundary Layers-1968 AFOSR-IFP Stanford Conference, Vol-I, p. 177 (also Ing.-Archiv 38 (1969), pp. 212-222).

26. Rotta, J.C., "FORTRAN IV - Rechenprogramm fuer Grenzschichten bei kompressiblen ebenen und achsensymmetrischen Stroemungen," Deutsche Luft-und Raumfahrt, Forschungsbericht 71-51 (1971).

27. Stanewski, E. and Thiede, P., "Boundary Layer and Wake Measurements in the Trailing Edge Region of a Rear-loaded Transonic Airfoil," DEA-Meeting on Viscous and Interacting Flow Field Effects, Meersburg/Bodensee, 1979.